

SVAIR SVENVIRO

**1D/2D/3D FINITE ELEMENT
PORE-AIR FLOW MODELING**

Verification Manual

**Written by:
The Bentley Systems Team**

Last Updated: Wednesday, August 28, 2019

Bentley Systems Incorporated

COPYRIGHT NOTICE

Copyright © 2019, Bentley Systems, Incorporated. All Rights Reserved.

Including software, file formats, and audiovisual displays; may only be used pursuant to applicable software license agreement; contains confidential and proprietary information of Bentley Systems, Incorporated and/or third parties which is protected by copyright and trade secret law and may not be provided or otherwise made available without proper authorization.

TRADEMARK NOTICE

Bentley, "B" Bentley logo, SoilVision.com, SoilVision logo, and SOILVISION, SVSLOPE, SVOFFICE, SVOFFICE 5/GE, SVOFFICE 5/GT, SVOFFICE 5/WR, SVSOILS, SVFLUX, SVSOLID, SVCHEM, SVAIR, SVHEAT, SVSEISMIC and SVDESIGNER are either registered or unregistered trademarks or service marks of Bentley Systems, Incorporated. All other marks are the property of their respective owners.

1	INTRODUCTION	4
2	TWO-DIMENSIONAL STEADY-STATE AIR FLOW	5
2.1	BAEHR & HULT (1991)	5
3	TWO-DIMENSIONAL TRANSIENT AIR FLOW	8
3.1	CONVECTIVE AIRFLOW IN EMBANKMENT (GOERING, 1999)	8
3.2	CHIMNEY VENTING	14
4	ONE-DIMENSIONAL AIR FLOW	18
4.1	TOUMA AND VAUCLIN (1985)	18
5	REFERENCES	26

1 INTRODUCTION

The word "Verification", when used in connection with computer software can be defined as "the ability of the computer code to provide a solution consistent with the physics defined by the governing partial differential equation, PDE". There are also other factors such as initial conditions, boundary conditions, and control variables that also affect the accuracy of the code to perform as stated.

"Verification" is generally achieved by solving a series of so-called "benchmark" problems. "Benchmark" problems are problems for which there is a closed-form solution or for which the solution has become "reasonably certain" as a result of long-hand calculations that have been performed. Publication of the "benchmark" solutions in research journals or textbooks also lends credibility to the solution. There are also example problems that have been solved and published in User Manual documentation associated with other comparable software packages. While these are valuable checks to perform, it must be realized that it is possible that errors can be transferred from one's software solution to another. Consequently, care must be taken in performing the "verification" process on a particular software package. It must also be remembered there is never such a thing as complete software verification for "all" possible problems. Rather, it is an ongoing process that establishes credibility with time.

Bentley Systems takes the process of "verification" most seriously and has undertaken a wide range of steps to ensure that the SVAIR software will perform as intended according to the theory of saturated-unsaturated air flow.

The following models represent comparisons made to textbook solutions, hand calculations, and other software packages. We at Bentley Systems are dedicated to providing our clients with reliable and tested software. While the following list of example models is comprehensive, it does not reflect the entirety of models, which may be posed to the SVAIR software. It is our recommendation that water balance checking be performed on all model runs prior to presentation of results. It is also our recommendation that the modeling process moves from simple to complex models with simpler models being verified through the use of hand calculations or simple spreadsheet calculations.

2 TWO-DIMENSIONAL STEADY-STATE AIR FLOW

The steady-state model is used to compare SVAIR results to those recorded in a study by Baehr & Hult (1991).

2.1 BAEHR & HULT (1991)

Baehr & Hult (1991), present two analytical solutions for steady-state axisymmetric airflow to a single well that is partially screened in the unsaturated zone. Input data were collected from a series of pneumatic tests. One model considers a stratum of relatively low air conductivity, separating the stratum in which the well is completed from the atmosphere. In the other scenario, there is no separating stratum between the material layer and the atmosphere. This second analytical model with no separated stratum as presented by Baehr & Hult has been created in SVAIR and is presented below.

Project: WellPumping
Model: BHuzPeq

2.1.1 Model Description

In this scenario, a single material layer is present and is exposed to the atmosphere. A well has been drilled to a depth of 2.88 m and a horizontal water table existed at a depth of 3.37 m.

Axisymmetric Model Geometry:

Well depth	= 2.88 m
Well screen height	= 0.60 m
Well radius	= 0.12 m
Model radius	= 20.00 m
Model depth	= 3.37 m

Boundary Conditions:

Ground Surface	= 0 kPa (gauge pressure)
Well screen side	= Normal Flux Expression of 0.14 m/s
Model base	= Zero Flux (water table)
Wellbore	= Zero Flux
Model side	= Zero Flux

Material Properties:

Intrinsic Permeability	= $1.4 \times 10^{-10} \text{ m}^2$
Vertical anisotropy ratio	= 0.31

An initial air pressure of 0 kPa is applied to entire material and an atmospheric pressure of 101.46 kPa was set in the model.

2.1.2 Results and Discussion

Figure 1 through Figure 4 show the normalized air pressure versus the radial distance from the pumping well at various depths. The square symbols represent the values obtained from the field tests. The dashed line indicates the analytical results. The results of the SVAIR analysis are presented as the solid line and are in good agreement with both the analytical and field results.

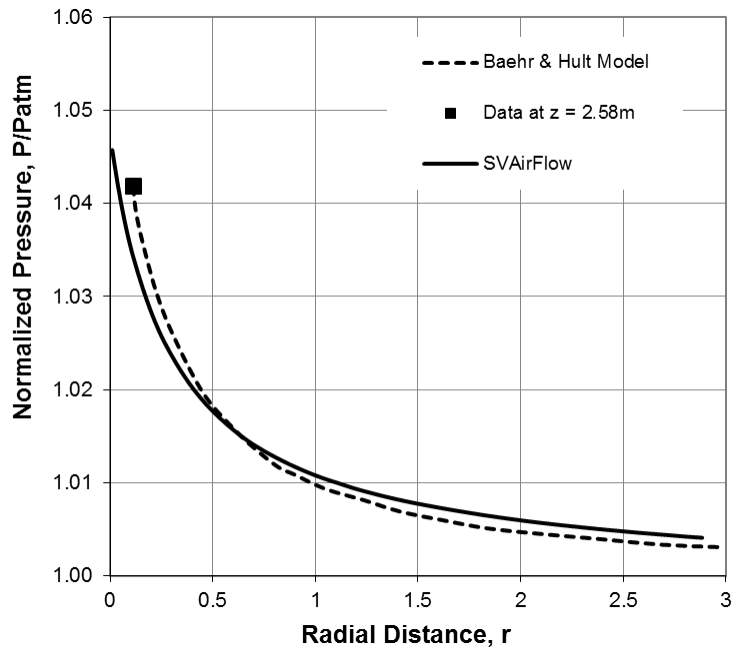


Figure 1 Normalized pressure as a function of cylindrical coordinates (r, z) in the upper unsaturated zone for $z = 2.58m$

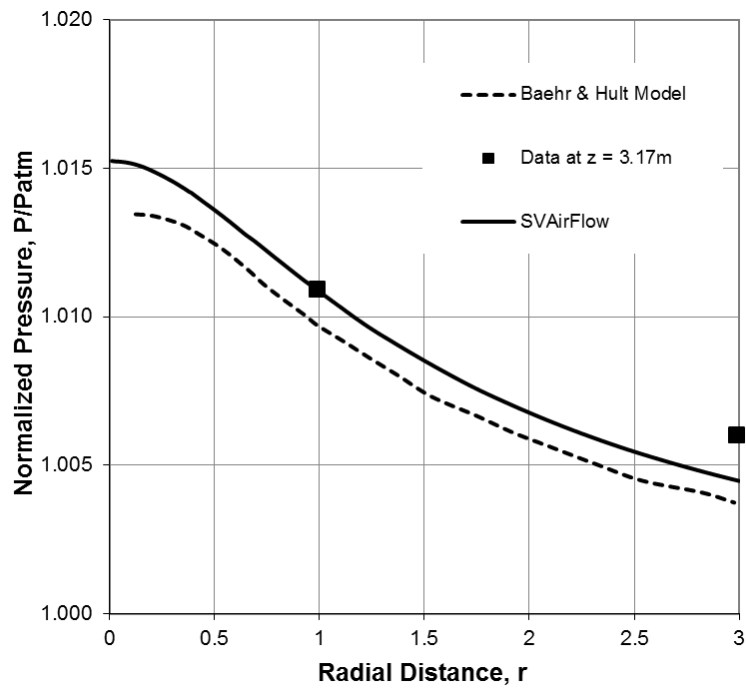


Figure 2 Normalized pressure as a function of cylindrical coordinates (r, z) in the upper unsaturated zone for $z = 3.17m$

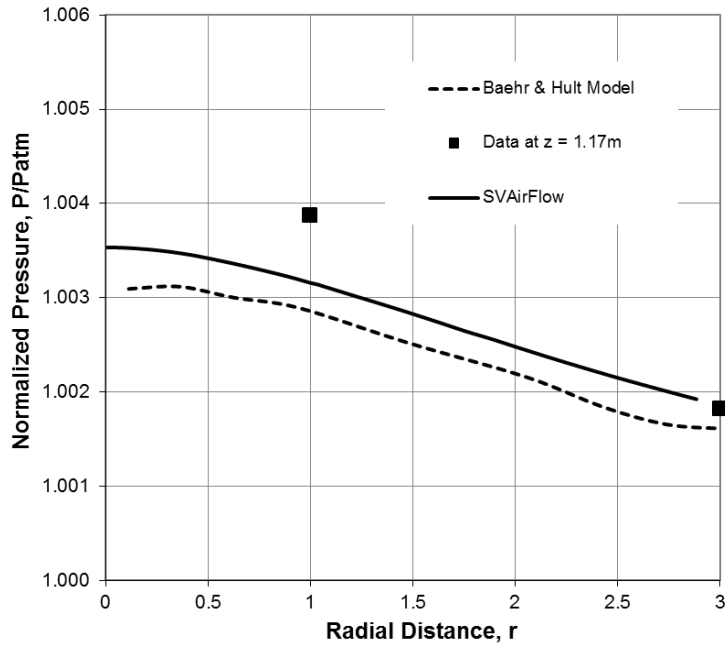


Figure 3 Normalized pressure as a function of cylindrical coordinates (r, z) in the upper unsaturated zone for z = 2.17m

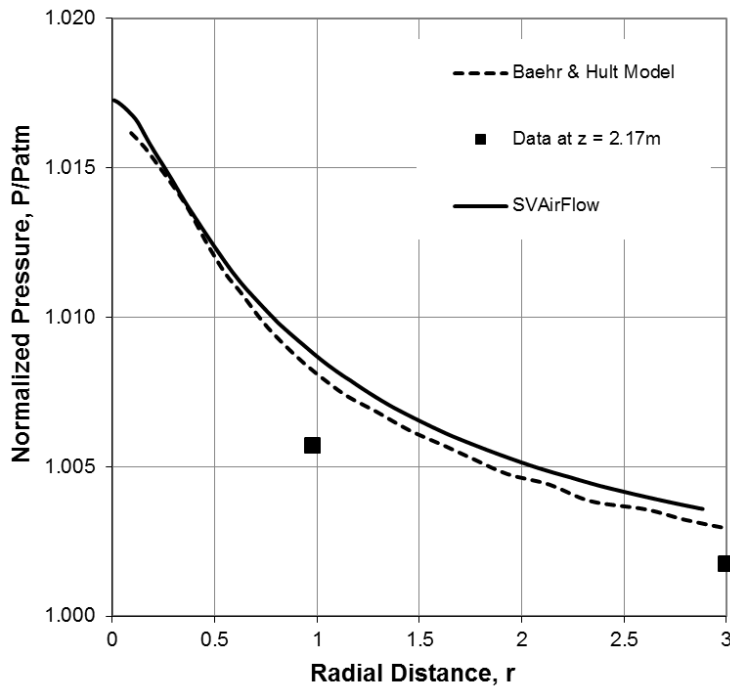


Figure 4 Normalized pressure as a function of cylindrical coordinates (r, z) in the upper unsaturated zone for z = 1.17m

3 TWO-DIMENSIONAL TRANSIENT AIR FLOW

3.1 CONVECTIVE AIRFLOW IN EMBANKMENT (GOERING, 1999)

Goering (1999), Sun et al. (2007), and Lebeau (2009) have conducted the numerical simulation of cooling an embankment using natural convection. The intent is to protect railway or roadway construction from thawing in permafrost areas. This example presents the characteristics of air flow and temperature distribution as governed by natural convection within the embankment using the SVAIR/SVHEAT software.

Project: Geothermal
 Model: Embankment_Convective_Airflow

3.1.1 Model Description

The model geometry of the right half of a symmetric roadway is shown in Figure 5. The embankment is constructed with a ballast type of material that has high air permeability. The pore-air in the embankment is allowed to approach equilibrium with the surrounding atmosphere. The ambient temperature changes with time, as described in equation [1]. The ground foundation is assumed to be uniform silt material with high water content. On the natural ground surface, the air transfer on the boundary is assumed to be impermeable, and the ambient temperature varies with time by equation [2]. The air is assumed to be incompressible in natural convection.

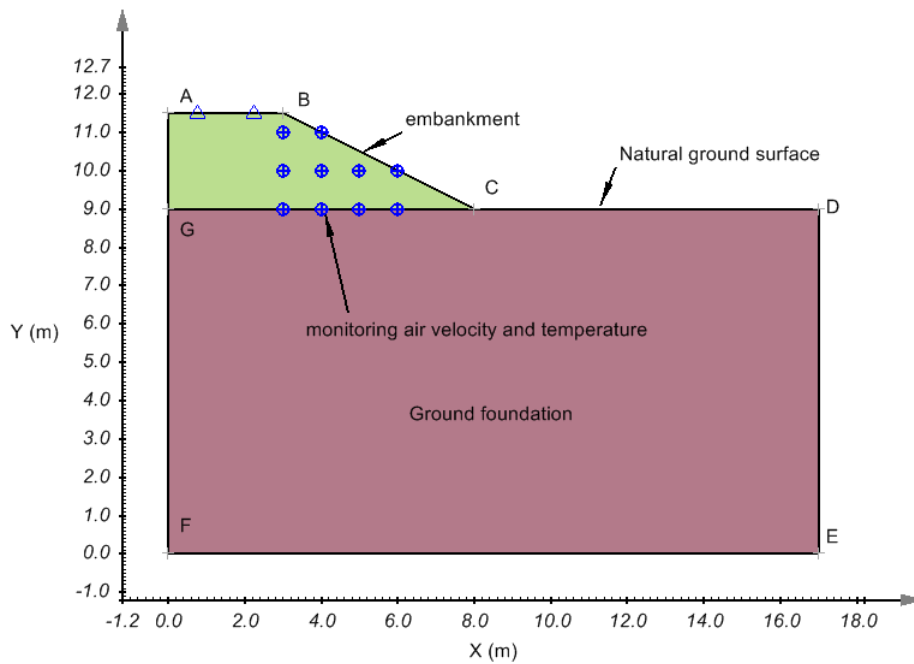


Figure 5 Model Geometry to simulate convective airflow in the embankment

Boundary Conditions:

Goering (1999) presented the empirical equations [1], [2] and [3] to describe the ambient temperatures change at the embankment surface (AB and BC), and ground surface CD. These applied temperatures were determined based on measured ambient temperature using the n-factor method (Goering, 1999). The embankment surfaces AB and BC are impermeable with zero flux boundary conditions. Table 1 contains the remaining boundary conditions for the model.

$$T_{ab} = 1.1 - 26.1 \cos\left(\frac{2\pi}{365}(t-9)\right) \quad [1]$$

$$T_{bc} = 2.7 - 20.9 \cos\left(\frac{2\pi}{365}(t-9)\right) \quad [2]$$

$$T_{cd} = -1.9 - 10.0 \cos\left(\frac{2\pi}{365}(t - 9)\right) \quad [3]$$

$$\rho = \rho_o (1 - \beta(T - T_o)) \quad [4]$$

where:

- $T_{ab,bc}$ = temperature used to apply the embankment surface AB and BC, °C,
- T_{cd} = temperature used to apply the natural ground surface CD, °C,
- t = time, day,
- ρ_o = air density at a reference temperature, kg/m^3 ,
- g = gravitational acceleration, m/s^2 ,
- y = elevation relative to the ground surface, m ,
- β = air expansion coefficient, $1/^\circ C$, $\beta = 1 / (237.15 + T)$,
- T_o = a reference temperature, 20 °C.

Table 1 Boundary conditions for convective air-flow model

Application	Boundary	Boundary Type	Value	unit
SVHEAT	AB and BC	Temperature expression	$T_{ab,bc}$ (see equation [1] and [2])	°C
	CD	Temperature expression	T_{cd} (see equation [3])	°C
	DE	Zero flux		
	EF	Flux expression	5184	J/day-m ²
	FG-GC-GA	Zero flux		
SVAIR	AB and BC	Zero flux		
	CD-DE-EF-FG-GC-GA	Zero flux		

Initial Conditions:

- Temperature: 2 °C,
- Pore (gauge) air pressure u_a : 0 kPa.

3.1.2 Material Properties

The main properties of the material used in the model are based on the values from Goering (1999), as shown in Table 2.

Table 2 Material properties used in convective air-flow model

Material	Properties	Method	Value	Unit
Embankment	Thermal conductivity	Constant	29894.4	J/day-°C
	Heat capacity	Constant	1.02×10 ⁶	J/m ³ -°C
	SFCC	None		
	Porosity		0.35	
	Volumetric water content		0	m ³ /m ³
	Air conductivity	Intrinsic permeability		6.30×10 ⁻⁷
Natural ground	Thermal conductivity	Johansen	25	%
	Dry density		1442	kg/m ³
	Quartz content		25	%
	SFCC	Multi-linear estimation		
	Porosity		0.45	
	Volumetric water content		0.45	m ³ /m ³
	Air conductivity	Intrinsic permeability		1.00×10 ⁻¹⁰

The air conductivity of a material in airflow is calculated based on air intrinsic permeability and air dynamic viscosity that is the function of air temperature. The thermal conductivity in heat transfer is calculated using the Johansen approach for the given quartz content. Please see **SVAIR Theory Manual** and **SVHEAT Theory Manual** for the detailed description on how the theoretical formulation makes use of the material properties.

3.1.3 Results and Discussion

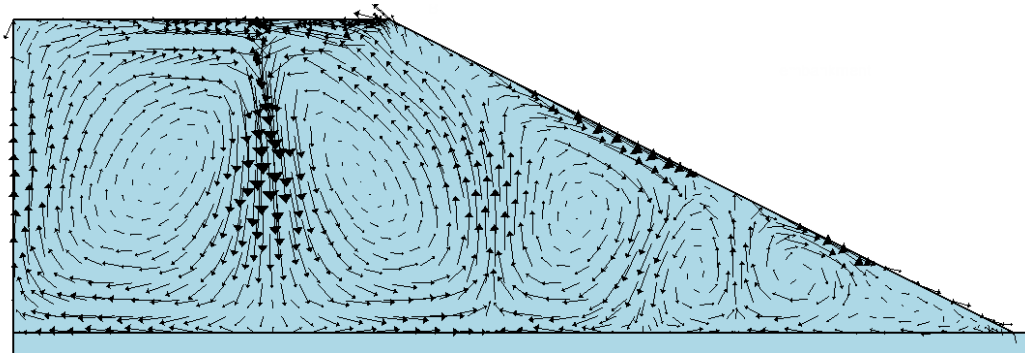
The model is simulated for 21 years to eliminate the effect of the initial condition on the temperature in the ground foundation. The following briefly discusses and compares the results with other software.

3.1.3.1 The patterns of convective air flow in the embankment

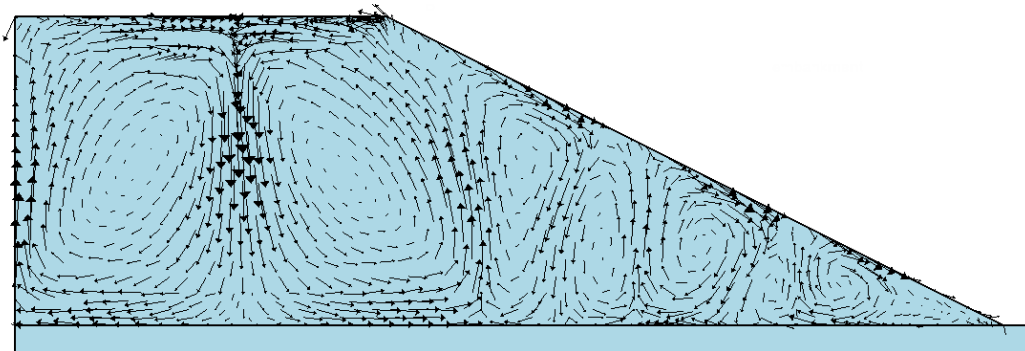
During winter, the cool and heavy air at the embankment surfaces sink into the embankment. This happens because the air density increases with the decrease in temperature. The warm air then rises up from the lower region in the embankment forming circulation cells and this process is called natural convection, as illustrated in Figure 6. The onset of natural convection depends on several parameters such as temperature differences between surface and the base of the embankment and permeability of the material. In this modelling, the onset occurs between October and November. After that time the intensity of convective airflow increases with the decrease in temperature until January. The convective flow reduces with the increase in temperature after the end of January (see Figure 6). During the summer, because the temperature on the embankment surface is higher than the temperature at the lower region in the embankment, a small amount of convective airflow occurs in the embankment (Figure 7).

3.1.3.2 Compare convective flow patterns with results from others

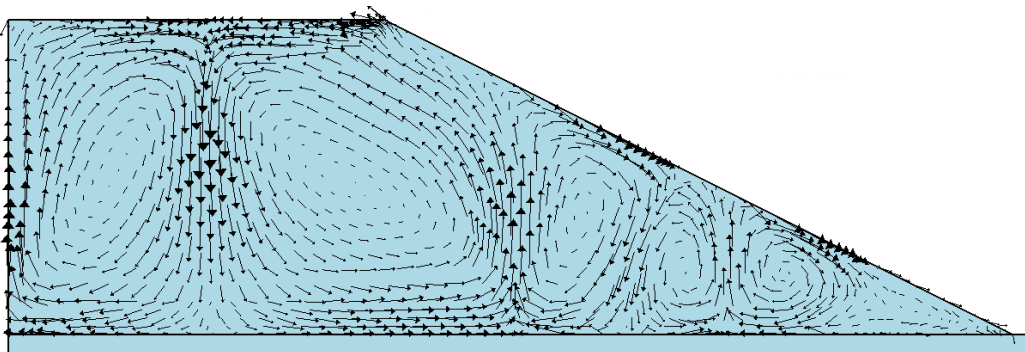
Figure 6 and Figure 7 are the airflow simulated from SVAIR/SVHEAT, and Figure 8 is from Goering (2003). It can be seen from Figure 6 and Figure 8 that the patterns of convective airflow at different times are very similar. It should be noted that the figures from Goering (2003) are presented only as a comparison of the flow pattern. An exact comparison to the flow vectors is not possible as Goering did not publish enough specifics of the modeling process. As illustrated in Figure 6, multi-convection cells are formed in wintertime. For the two neighboring convective cells, if one flows clockwise, another must move counter-clockwise. This characteristic of natural convection was also discussed in other research (Chen et al., 2008).



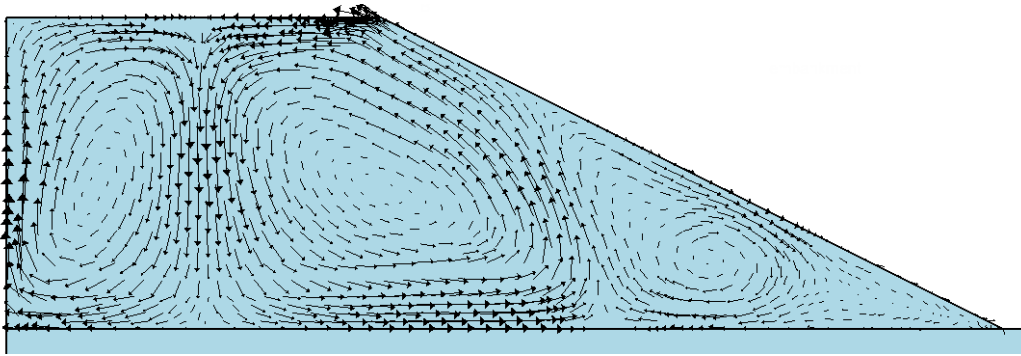
Mean air velocity = 32.70 m/hr



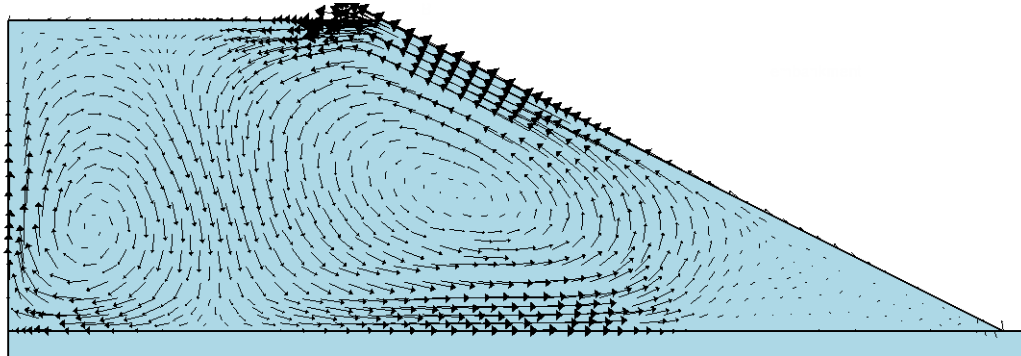
Mean air velocity = 47.33 m/hr



Mean air velocity = 43.00 m/hr

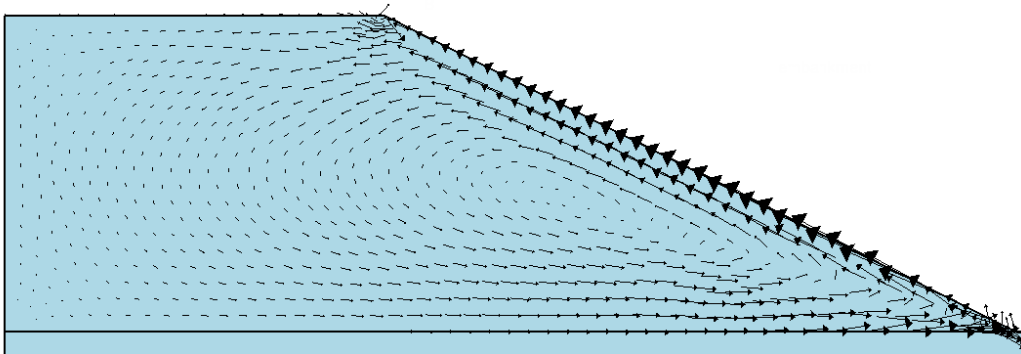


Mean air velocity = 28.37 m/hr

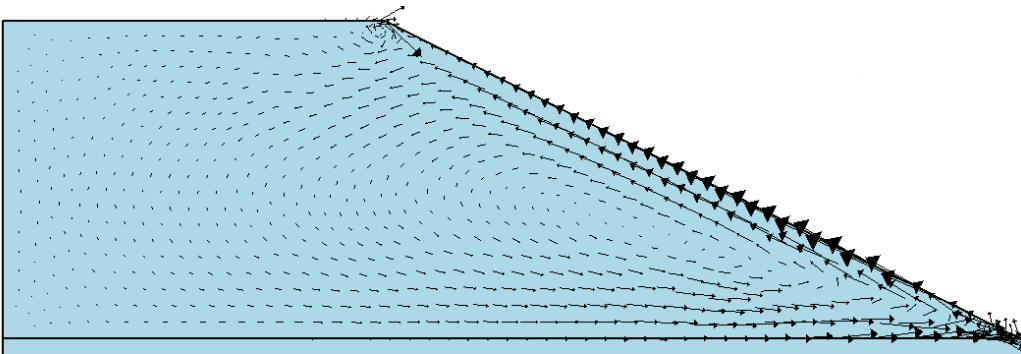


Mean air velocity = 12.50 m/hr

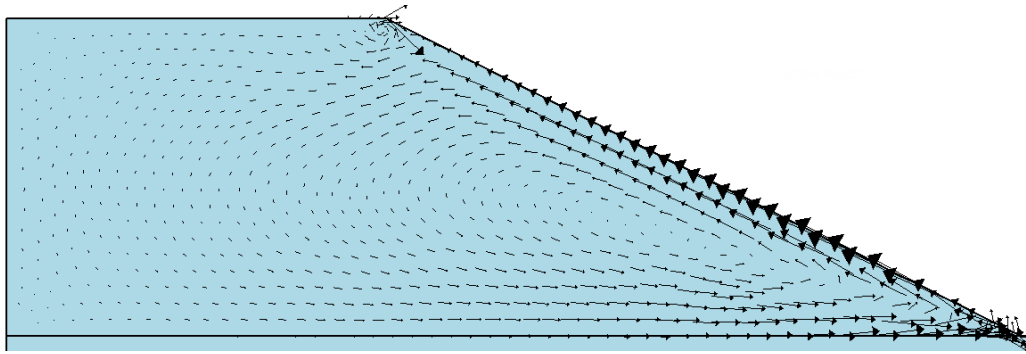
Figure 6 Patterns of convective airflow during winter, from November to March of year 3



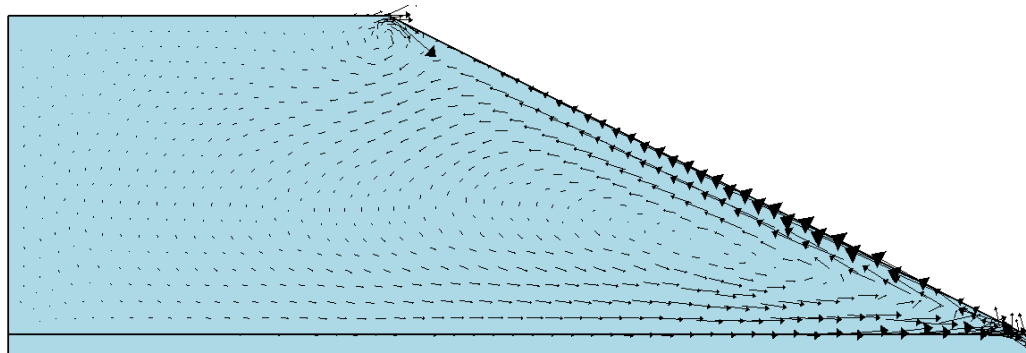
Mean air velocity = 14.50 m/hr



Mean air velocity = 17.80 m/hr



Mean air velocity = 16.90 m/hr



Mean air velocity = 12.60 m/hr

Figure 7 Patterns of convective airflow during summer, from May to August

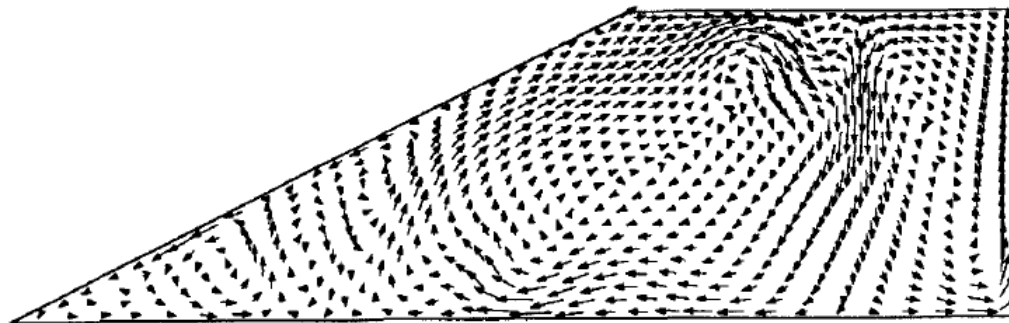


Figure 8 Patterns of convective airflow presented by Goering (1999), in January

3.1.3.3 Temperature distributions with natural convection

The maximum soil temperature at the base of the embankment is of particular interest in evaluating the embankment stability in a permafrost area. The construction of a railway or highway in a permafrost area is performed above the permafrost layer. If the soil temperature below the ground surface of the embankment is above the soil freezing point, thaw settlement of the permafrost results in damage to the embankment. It can be seen that the maximum soil temperature during the summer (in July) at the base of the embankment is changed from the initial value of 2 °C to 0 °C. The embankment base is cooling due to the effect of natural convection. Figure 9 illustrates the temperature contours in July and January compared to the similar temperature profiles from Goering (2003) is shown in Figure 10.

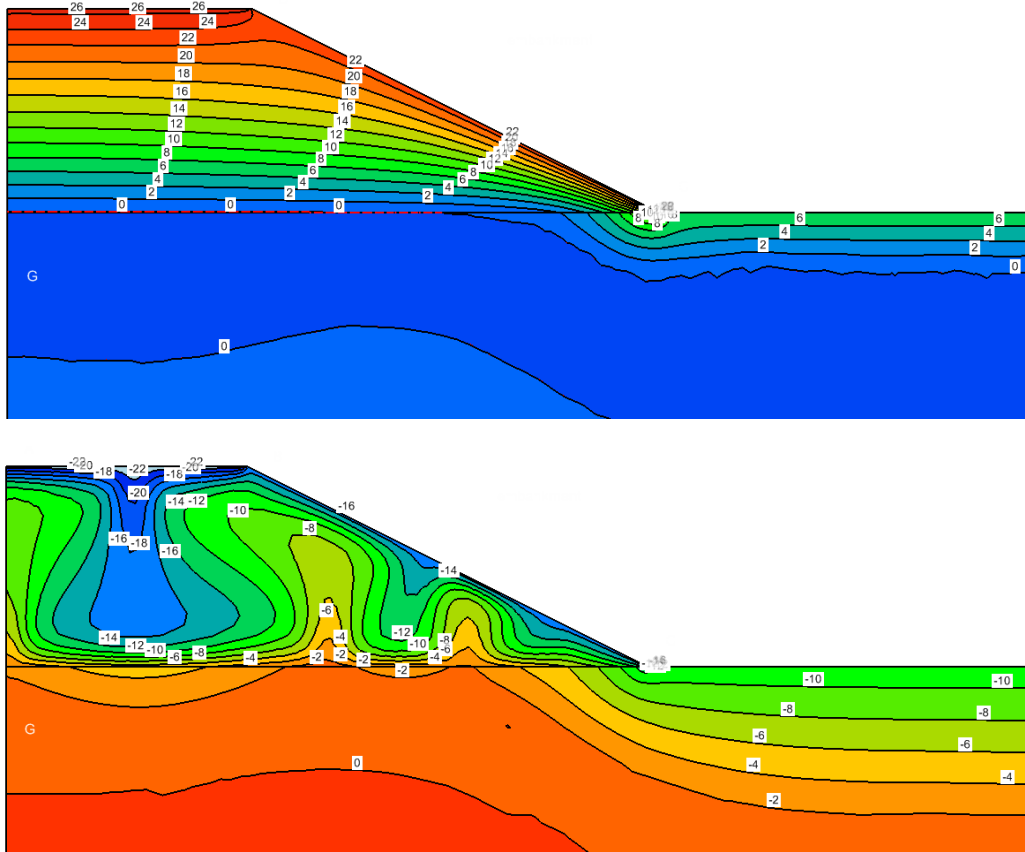
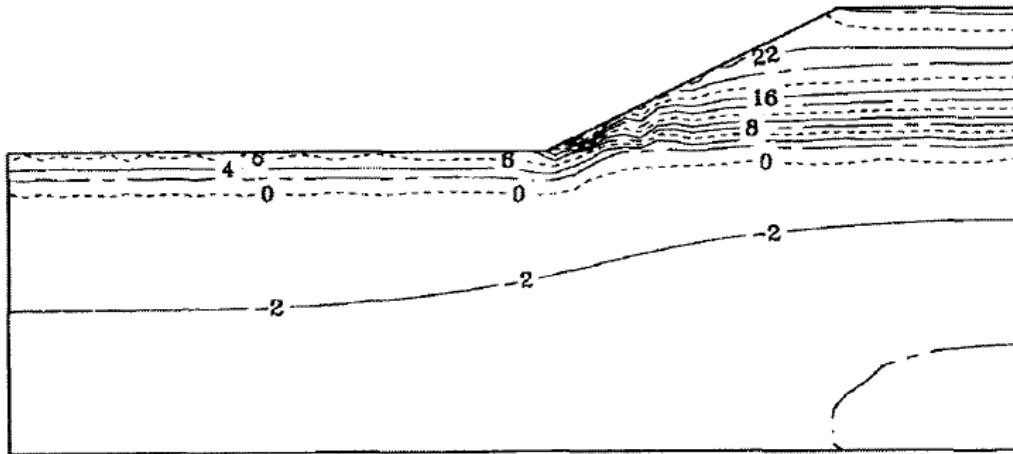


Figure 9 Temperature contours within the embankment in July and January



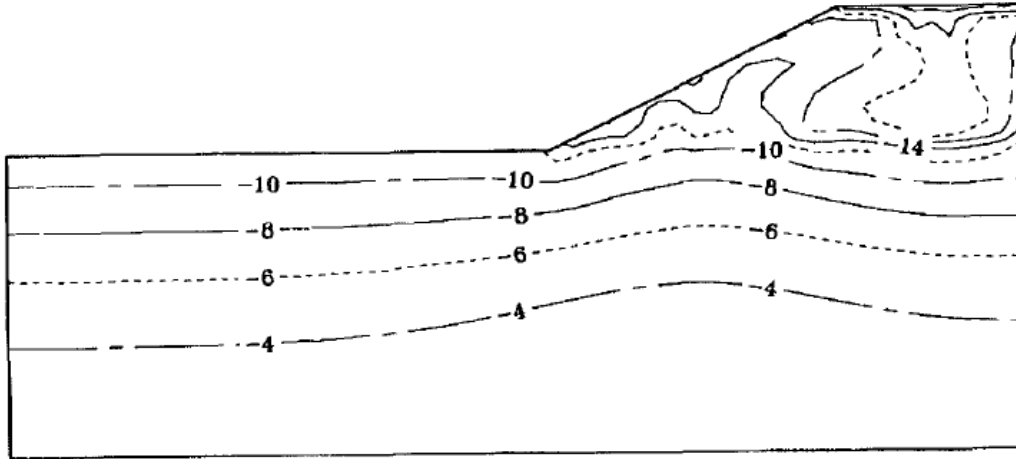


Figure 10 Temperature contours within the embankment in July and January (Goering, 1999)

3.2 CHIMNEY VENTING

The physics of chimney venting are based on the stack effect, in which warm lighter air raises up and out and cold air is drawn in and there is a buoyancy effect or natural air convection. This difference in air density can cause temperature and/or moisture difference between the inside and outside of the chimney. To model this, both SVAIR and SVHEAT need to be coupled.

Project: Geothermal
Model: Chimney_Venting

3.2.1 Model Description

The geometry of the model is shown in Figure 11 and it shows the areas, where air is drawn in and moved out the chimney and the heated base where cold air is heated and rises up.

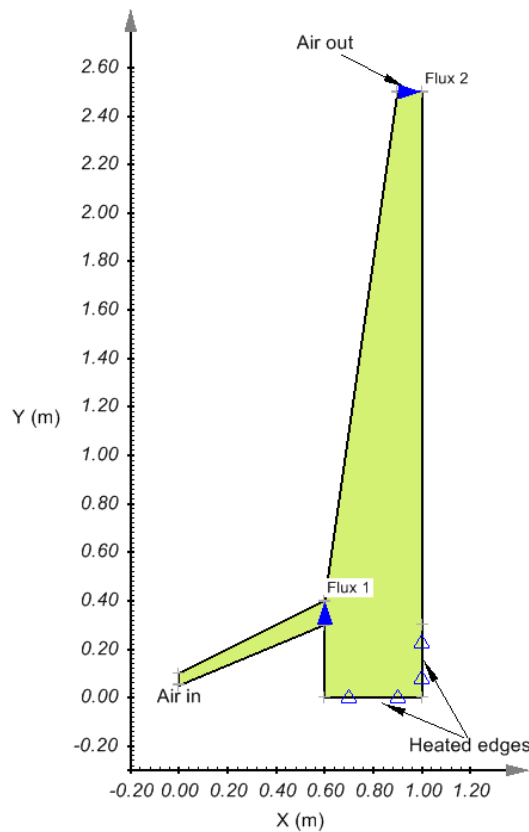


Figure 11 Model Geometry

Initial conditions:

This is a transient model and therefore initial conditions are needed for both SVAIR and SVHEAT.

Temperature: 13 °C,
 Pore (gauge) air pressure u_a : 0 kPa.

Boundary conditions:

Pore air pressure: 0 kPa at Air-out edge
 0.02 kPa at Air-in edge
 Temperature: if $t \leq 500$ then $0.574 * t + 13$ else 300

The temperature at the heated edge rises gradually from 13 °C to 300 °C over 500 seconds. Other edges have a zero-flux boundary condition.

3.2.2 Material Properties

Material properties are shown in Table 3 and the degree of air saturation is 99 %. Air density is calculated based on the current air temperature and pressure. The dynamic viscosity of air is a function of temperature.

Table 3 Material properties used in convective air-flow model

Properties	Method	Value	Unit
Thermal conductivity	Constant	2.40	W/m-°C
Heat capacity	Constant	1173	J/m ³ -°C
Air conductivity	Constant	3.0	m/s

3.2.3 Results and Discussion

The model was run for 1000 seconds. Steady-state natural air convection has been established. Figure 12 shows the air velocity pattern after 1000 seconds. This figure indicates that the cold-heavy intake air first sinks into the heated edges then it is heated and rises up. The rising hot air is lighter.

Figure 13 shows the temperatures at 1000 seconds and the contour indicates cold temperature near the air intake and warmer temperatures near the heated edges and along the air outlet. The temperature and air velocity results of SVAIR are very similar to AIR/W (Figure 13, right) (GEO-SLOPE, 2012).

Figure 14 shows the normal flux rates at the flux sections, Flux-1 and Flux-2. This figure shows that not until 500 seconds, air flows out of the inlet and comes in from the outlet at a decreasing rate until 500 seconds. After 500 seconds, the air direction reverses and becomes steady state afterward. This volume fluxes are comparable to AIR/W results (GEO-SLOPE, 2012). Similarly, the cumulative fluxes are shown in Figure 15.

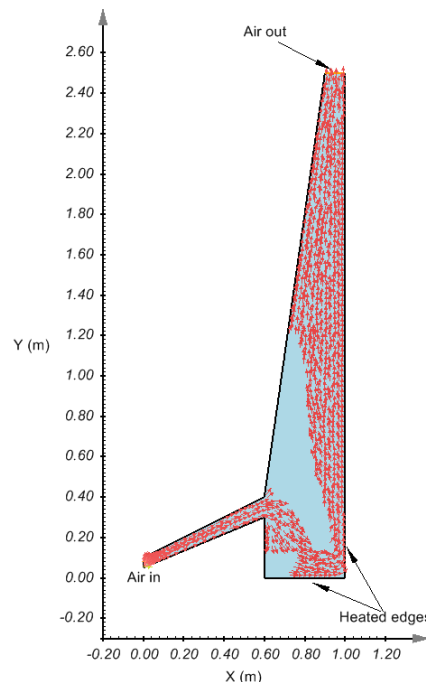


Figure 12 Air velocity pattern

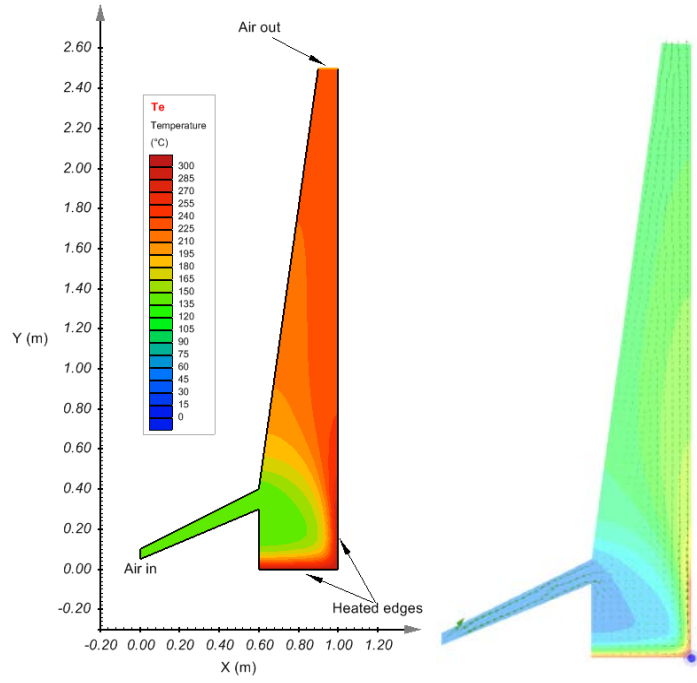


Figure 13 Temperature contour, SVAIR (left) and AIR/W (right)

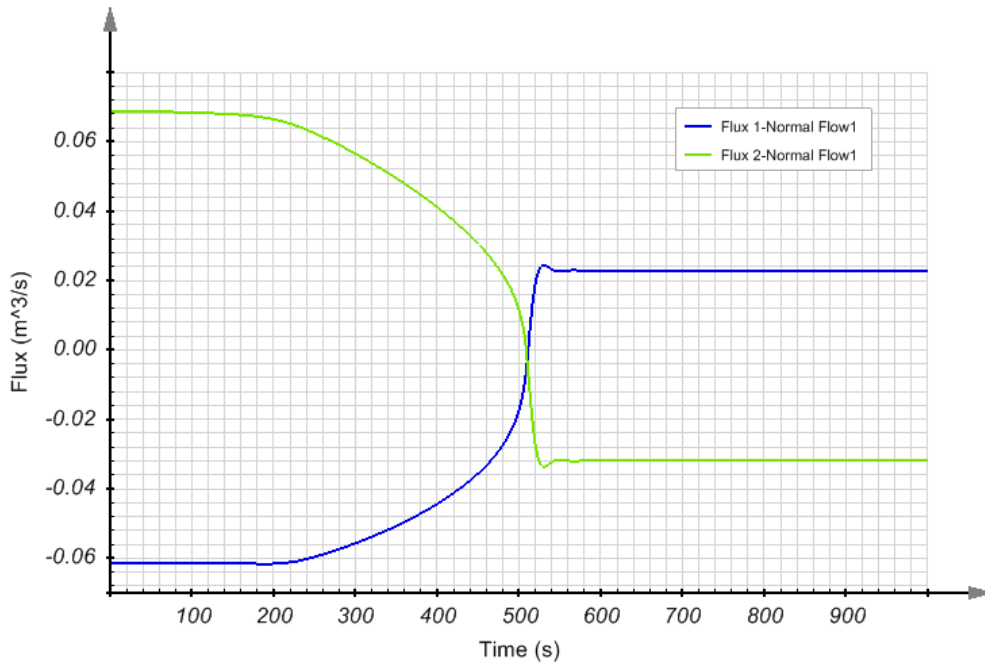


Figure 14. The variation of normal flux rate in m³/s at Flux-1 and Flux-2 sections

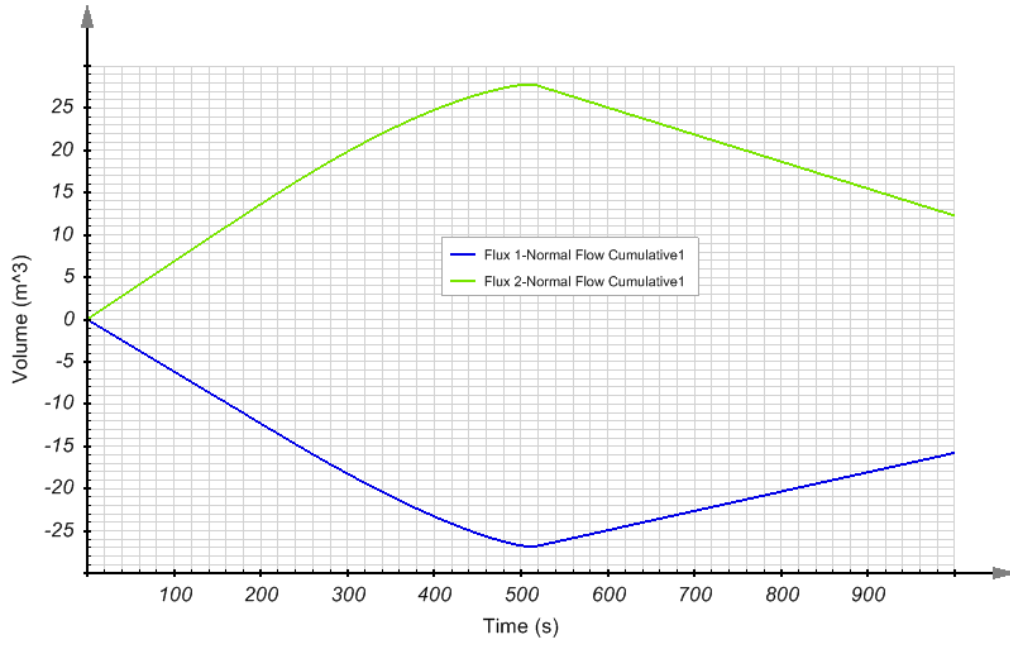


Figure 15. Cumulative flux rate in m³ at Flux-1 and Flux-2 sections

4 ONE-DIMENSIONAL AIR FLOW

4.1 TOUMA AND VAUCLIN (1985)

Touma and Vauclin (1985) conducted experimental and numerical analysis of two-phase infiltration in an unsaturated soil column. This model is designed to use their experimental results for the verification of infiltration coupled with airflow using the SVAIR and SVFLUX software.

Project: Columns
 Model: Touma_1985

4.1.1 Model Description

The model is simulated using a vertical one-dimensional soil column. The model geometry is illustrated in Figure 16. The soil column has 1 m height. Initially, the soil column is unsaturated, and the pore air is connected to atmosphere. The lower end of the soil column does not allow air-flow. The upper end is open to the atmosphere. During the simulation, a constant water infiltration is applied at the upper end of the soil column. With the increase in the degree of wetting soil saturation, the air-flow movement is impeded in its attempt to escape from the upper end of soil column. It can be expected that the pore air pressure in the soil column will increase. The increasing pore air pressure will obstruct the water infiltration rate. The following initial conditions and boundary conditions are applied to simulate the interaction of air and water flow.

Figure 16 Model geometry to simulate airflow and infiltration

Initial Conditions:

Water head: 0 m for SVFLUX application
 Pore air pressure (gauge) u_a : 0 kPa for SVAIR application

Boundary Conditions:

Table 4. Boundary condition inputs

Test cases	Application	y-coordinate (m)	Boundary Type	Value	unit
Case 1: Light infiltration rate	SVFLUX	1.0	Normal flux	0.083	m/hr
		0	Zero flux		
	SVAIR	1.0	Air pressure	0	kPa
		0	Zero flux		
Case 2: Heavy infiltration rate	SVFLUX	1.0	Normal flux	0.166	m/hr
		0	Zero flux		

SVAIR	1.0	Air pressure	0	kPa
	0	Zero flux		

4.1.2 Material Properties

According to soil properties presented by Touma (1985), the soil water characteristic curve can be described with the van Genuchten equation, as illustrated in Figure 17, and the hydraulic conductivity changing with matric suction is approximated in Figure 18. The saturated volumetric water content is $0.316 \text{ m}^3/\text{m}^3$, and saturated hydraulic conductivity is about 0.154 m/hr . The function of air conductivity as the function of the degree of water saturation was given in Figure 19.

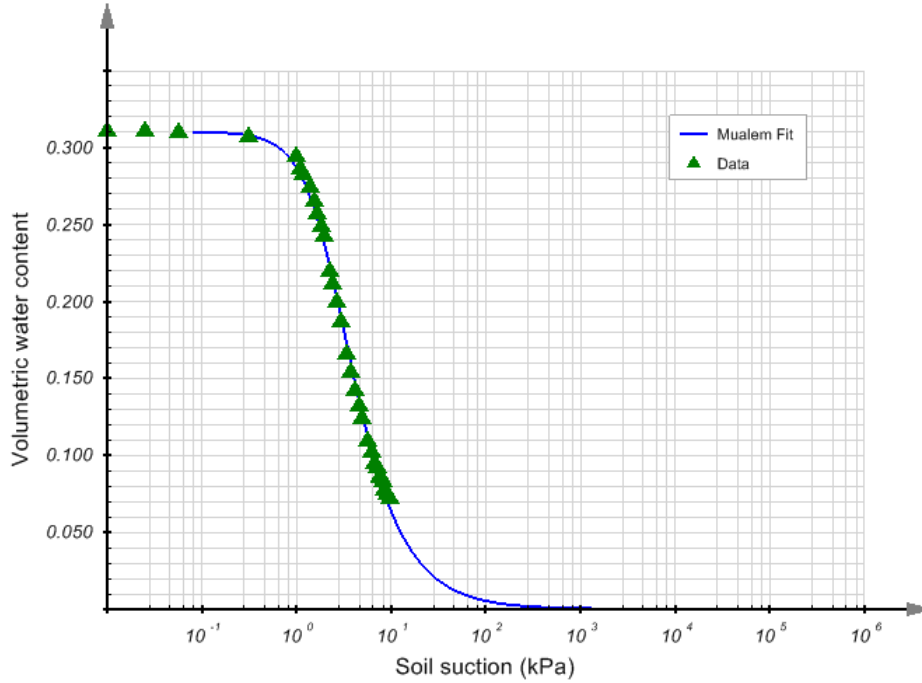


Figure 17 Soil water characteristic curve (SWCC) based on Touma experimental data (1985) and van Genuchten and Mualem estimation method

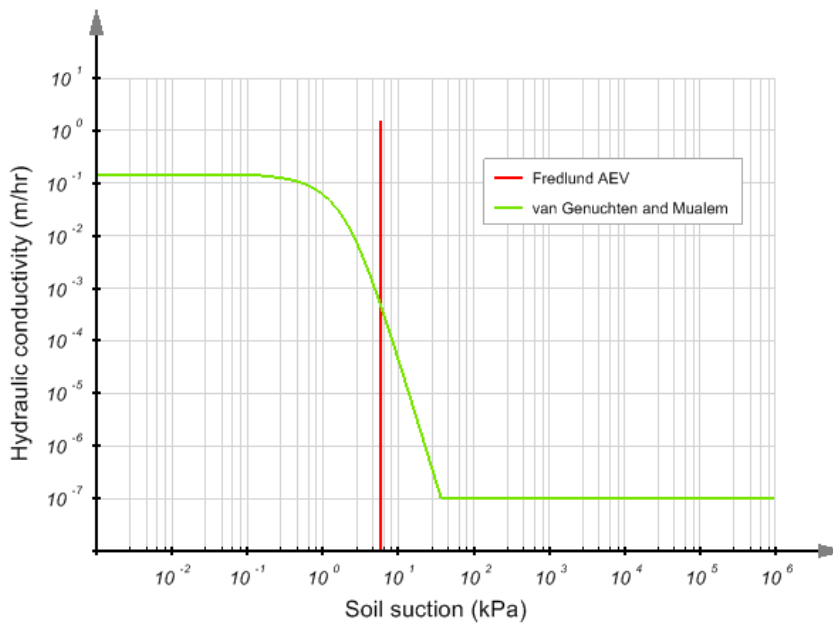


Figure 18 Hydraulic conductivity vs. soil matric suction based on Touma experimental data (1985), and van Genuchten and Mualem estimation method

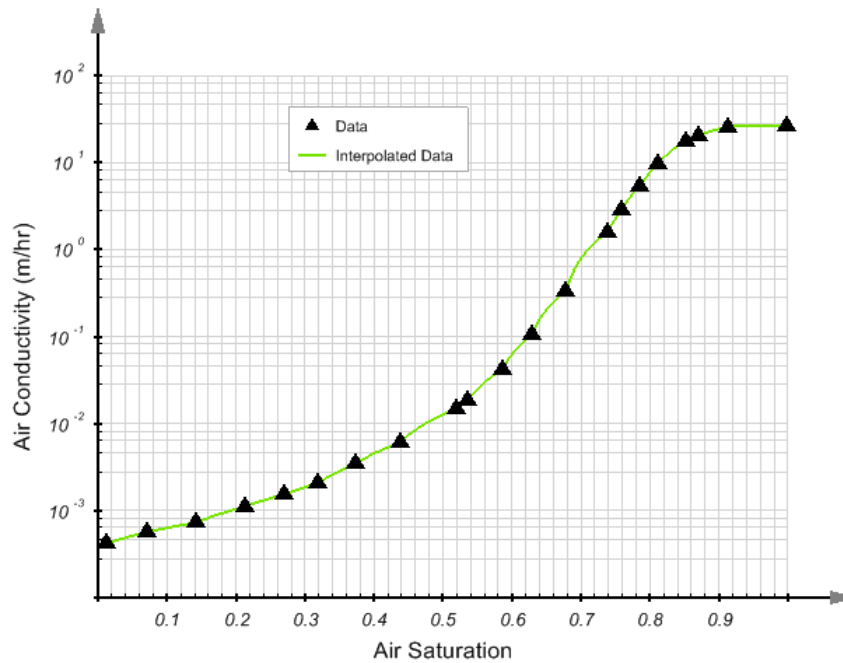


Figure 19 Air conductivity changing with the degree of water saturation based on Touma experimental data (1985) and Binning (1994)

4.1.3 Results and Discussion

The following sections present the results of the model simulation. The comparison of the simulation with other results obtained by Touma (1985) and Binning (1994) is included.

4.1.3.1 Air pressure build-up

As soil wets, the air conductivity decreases due to the increase in the degree of water saturation (see Figure 19). Consequently, the pore air pressure in the soil column will increase. Figure 20 illustrates the behavior of the build-up of pore air pressure with time at different elevations in the soil column.

Figure 21 illustrates the change of air pressure, u_a , water pressure, u_w , matric suction $u_a - u_w$, and water content at the elevation of $y = 0.78 \text{ m}$. The saturated hydraulic conductivity of the soil is approximately 0.154 m/hr . When a constant infiltration rate of 0.083 m/hr is applied at the upper end of the soil column, the pore air can escape from the upper end of the soil column, and the air pressure slowly increases (Figure 21a). When a higher infiltration rate of 0.166 m/hr is applied, the soil at the top of the soil column is saturated. The air pressure increases at a faster rate because the air escape path is blocked by the saturated soil as shown in Figure 21b. Please note that the matric suction $u_m = u_a - u_w$ becomes negative after the soil is over-saturated (Figure 21b). Figure 22 to Figure 24 further illustrate the profiles of air density, air pressure, and matric suction along the soil column at different times.

4.1.3.2 Comparison with results from Touma (1985) and Binning (1994)

Figure 25 is the comparison of the calculated water content profile in the soil column with the experimental results from Touma (1985). It can be seen from Figure 25 that the calculated water content profile is in a good agreement with the measured values.

Figure 26 shows the pore water and air pressure profile calculated from SVAIR and Figure 27 is the numerical result from Binning (1994). Comparison of Figure 26 with Figure 27 indicates that the calculations from SVAIR and Binning (1994) are very similar.

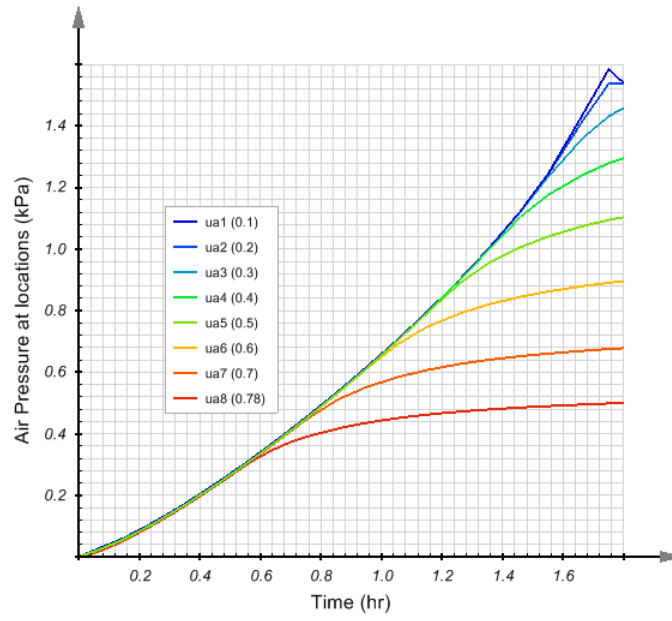
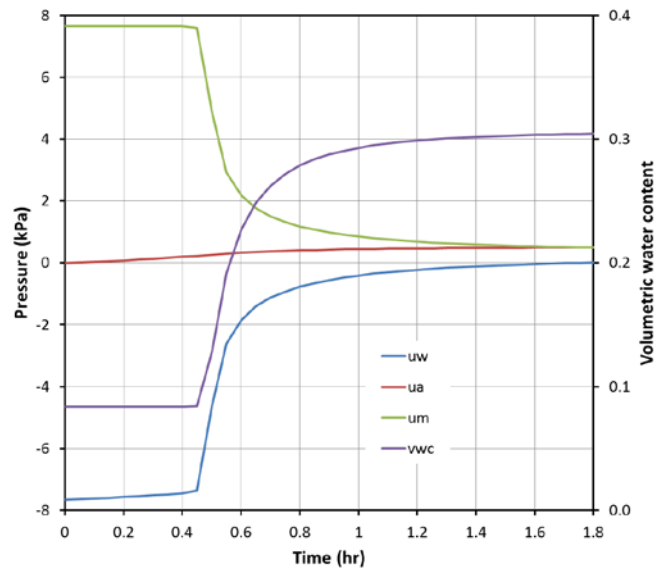


Figure 20 Air pressure build-up with water infiltration time



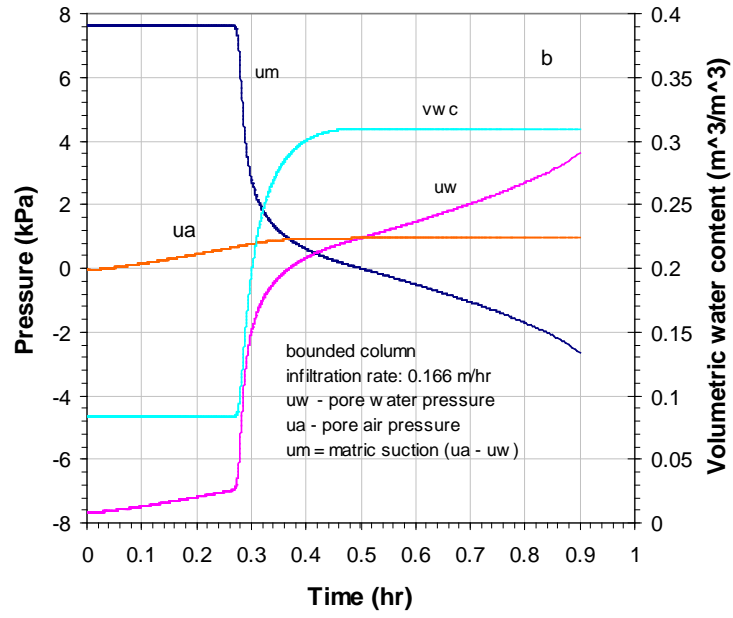


Figure 21 The change of pore water pressure, air pressure, matric suction, and volumetric water content with time at the elevation of $y = 0.78\text{ m}$ and at the different infiltration rates

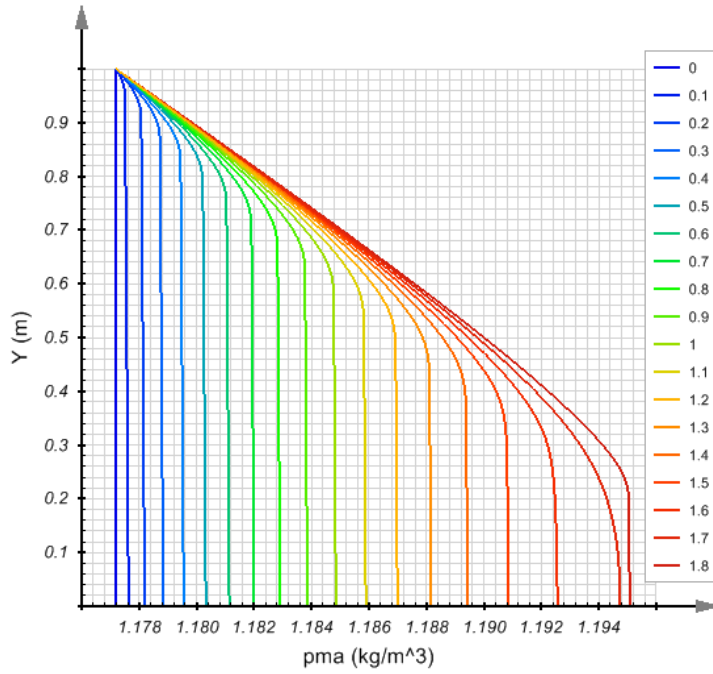


Figure 22 Air density profiles at different times for the bounded soil column at a filtration rate of 0.083 m/s

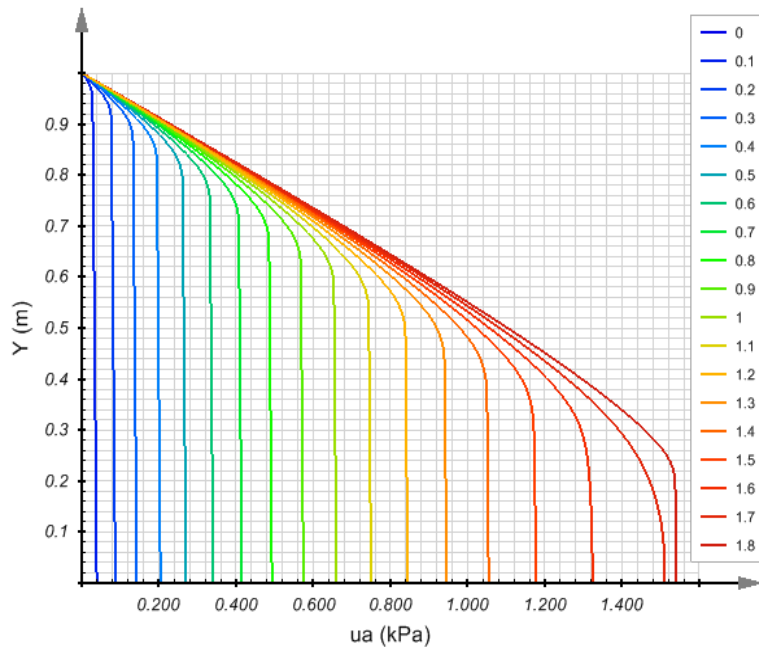


Figure 23 Air pressure (gauge) profiles at different times for the bounded soil column at a filtration rate of 0.083 m/s

s

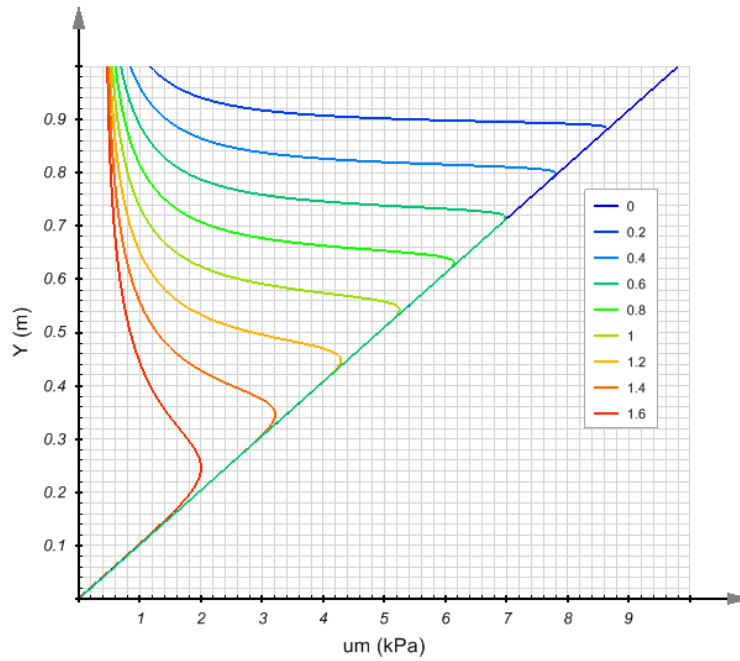


Figure 24 Matric suction, u_m , profiles at different times at a filtration rate of 0.083 m/s

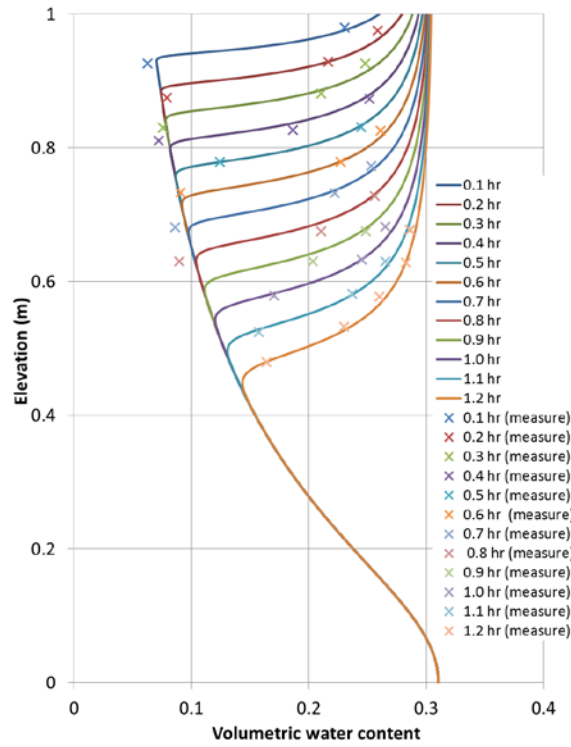


Figure 25 Calculation and measured data of water content at a filtration of 0.083 m/hr

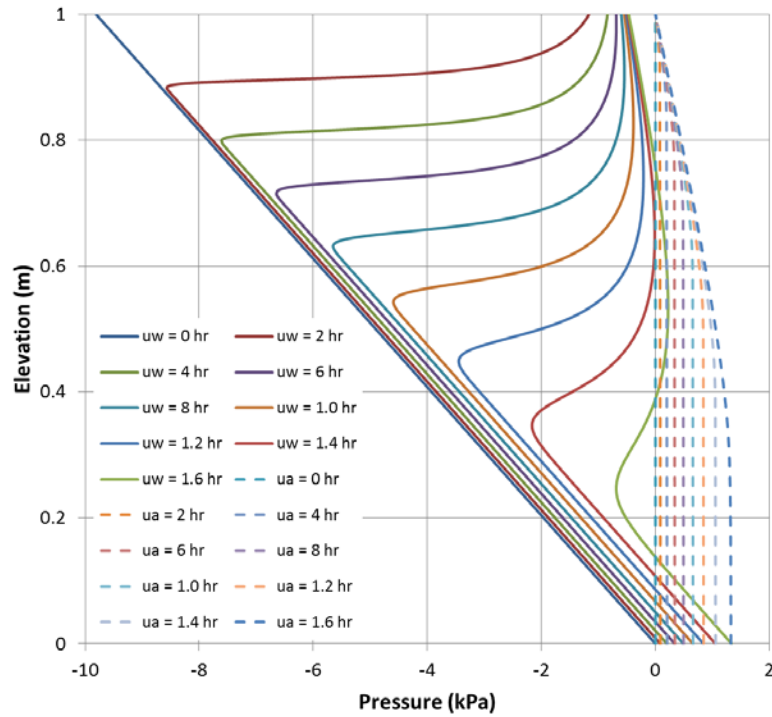


Figure 26 The profile of pore water and pore air pressure changing with time

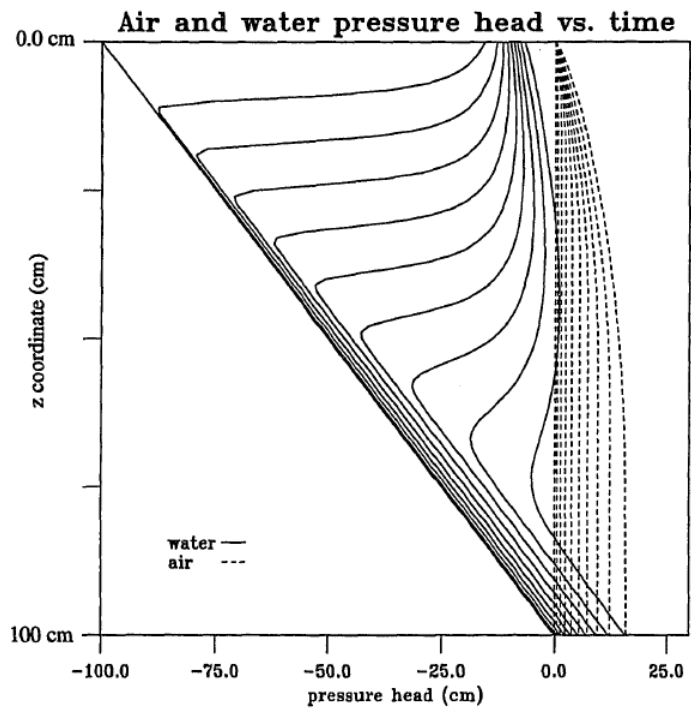


Figure 27 The profile of pore water and air pressure obtained from Binning (1994)

5 REFERENCES

- Baehr, A.E., and Hult, M.F. 1991. Evaluation of Unsaturated Zone Air Permeability Through Pneumatic Tests. *Water Resources Research*, 27(10): 2605-2617.
- Binning, P. 1994. Modeling unsaturated zone flow and contaminant transport in the air and water phases. Ph.D thesis, Princeton University 1994.
- Celia, M. and Pinning. 1992. A mass conservative numerical solution for two-phase flow in porous media with application to unsaturated flow. *Water Resources Research*. 28: 2819-2828.
- Chen, G., Sun, Z., and Niu, F. 2008. Application of the Roadbed Cooling Approach in Qinghai-Tibet Railway Engineering. *Cold regions science and technology*, 53: 241-258.
- FlexPDE 6 (2007). *Reference Manual*, PDE Solutions Inc., Spokane Valley, WA 99206.
- FlexPDE 7 (2017). *Reference Manual*, PDE Solutions Inc., Spokane Valley, WA 99206.
- Goering, D. J. (1999). Permeability effects on winter-time natural convection in gravel embankments. *Advances in Cold-Region Thermal Engineering and Sciences*. Vol. 533: pp 455-464.
- Lebeau, M., and Konrad J-M. 2009. Natural Convection of Compressible and Incompressible Gases in Undeformable Porous Media under Cold Climate Conditions. *Computer and Geotechnics*, 30: 435-445.
- Sun, B., Yang, L. and Xu, X. (2007). Onset and Evaluation on Winter-time Natural Convection Cooling Effectiveness of Crushed-rock Highway Embankment. *Cold regions science and technology*, 48: 218-231.
- GEO-SLOPE (2012). AIW/W – Chimney venting simulation.
- Touma, J., Vauclin, M. 1985. Experimental and Numerical Analysis of Two-Phase Infiltration in a Partially Saturated Soil. *Transport in Porous Media* 1(1985) 27-55.
- Zhan, X. 1995. Numerical Simulation of Two-Phase Flow and Solution Transport with Interphase exchange in Porous Media. *Communications in Numerical Methods in Engineering*, 12: 433-444.

This page has been left blank intentionally.